Journal of Materials Chemistry A

COMMUNICATION

View Article Online
View Journal | View Issue

Cite this: J. Mater. Chem. A, 2014, 2, 7680

Received 27th February 2014
Accepted 28th March 2014

DOI: 10.1039/c4ta01004c

www.rsc.org/MaterialsA

The design and construction of 3D rose-petal-shaped MoS_2 hierarchical nanostructures with structure-sensitive properties†

Han Zhu,[a] MingLiang Du,*[ab] Ming Zhang,[ab] MeiLing Zou,[a] TingTing Yang,[a] YaQin Fu[ab] and JuMing Yao[ab]

Rose-petal-shaped MoS_2 hierarchical nanostructures were designed and constructed using carbonized electrospun nanofibers as a template, which exhibit highly structure-sensitive properties for the hydrogen evolution reaction (HER). We first synthesized carbon nanofiber (CNF) mats by combining the electrospinning and carbonization processes, and then the CNF mats were used as a substrate for the direct growth of MoS_2 nanocrystals *via* the CVD method. By controlling the MoS_2 morphology at the nanoscale, we constructed evolutions in the structures and preferentially exposed more catalytically active edge sites, enabling improved performance for electrochemical catalytic activity. Because of their highly exposed edges and excellent chemical and electrical coupling to the underlying CNFs, MoS_2–CNF fiber mats exhibited excellent HER activity with a small overpotential of ~0.12 V and a small Tafel slope of 45 mV per decade. Our findings provide a feasible way to design and engineer advanced nanostructures for catalysis, electronic devices, and other potential applications.

Introduction

The rational design and construction of materials with structure-sensitive properties at the nanoscale is paramount in developing advanced nanomaterials. Novel properties may arise when the size of a material is decreased to the nanoscale and the dimensionality is lowered, due to quantum confinement effects and edge effects.[1–3] As a new member of the 2D material family, molybdenum disulfide (MoS_2) has recently been discovered to have a unique combination of optical, mechanical, electronic and chemical properties and is fundamentally and technologically intriguing.[1,2,4–6] Although traditionally used as an industrial hydrodesulfurization catalyst, MoS_2 is an exciting hydrogen evolution reaction (HER) catalyst that exhibits promising HER activity in crystalline or amorphous materials and molecular mimics.[5] However, its HER eletrocatalytic activity is currently limited by the density and reactivity of active sites, poor electrical transport, and inefficient electrical contact with the catalyst.[7]

Previous studies have reported that the HER activity stemmed from the sulfur edges of the MoS_2 plates, while the basal planes were catalytically inert.[5,8] As a result, tremendous efforts have been made to design and engineer the structures of MoS_2 catalysts with exposed active sites.[1,9] In addition, MoS_2 is a semiconductor whose poor bulk conduction and anisotropic electrical transport can limit overall catalytic efficiency. Previous studies reported MoS_2 catalysts supported on Au,[5] graphene,[8] graphite[7] and carbon paper,[10] which were prepared by physical vapor deposition or annealing of molybdate in H_2 or H_2S. In addition, various overpotentials (from 0.1 to 0.4 V) and Tafel slopes (from 41 to 120 mV per decade) have been reported.[5,7–10] Moreover, the morphology and distribution of the catalytically important edge sites of MoS_2 are found to be sensitive to preparation conditions, edge-attached promoter atoms, and interactions with support media.

Carbon nanotubes (CNTs) are widely used as substrates for the support of catalysts, and they have attracted a lot of attention in recent years as a result of their unique structure and wide potential application in electrochemical devices and energy conversion and storage devices.[11–14] Similar to CNTs, electrospun carbon nanofibers (CNFs), with wide application in electrochemical devices, are now at the cutting edge of materials science.[14–16] CNFs are composed of graphene layers that form stacked cones, while CNTs are composed of concentric hollow graphene cylinders.[15,16] Compared with CNTs, CNFs have several advantages, including qualitatively reproducible synthesis, controlled morphology, and larger functionalized surface area for the immobilization of molecules. Electrospinning is currently the only technique that allows the fabrication of continuous fibers with diameters down to a few nanometers.[16–18] In the present investigations, we have

[a]Department of Materials Engineering, College of Materials and Textile, Zhejiang Sci-Tech University, Hangzhou 310018, P. R. China

[b]Key Laboratory of Advanced Textile Materials and Manufacturing Technology, Zhejiang Sci-Tech University, Ministry of Education, Hangzhou 310018, P. R. China. E-mail: du@zstu.edu.cn; Tel: +86-571-86843255

† Electronic supplementary information (ESI) available. See DOI: 10.1039/c4ta01004c

developed a simple electrospun polyacrylonitrile nanofiber (PANF) based graphitization method to fabricate 1D CNFs that are composed of graphitic nanorolls and possess good conductivity and numerous active sites, which can serve as nuclear sites for the growth of MoS_2 nanocrystals.

Solution-phase production of MoS_2 by exfoliation or hydrothermal synthesis holds promise for large-scale production, and Zafiropoulou *et al.* have reported the deposition of MoS_2 material on CNTs and CNFs by *in situ* thermal decomposition of $(NH_4)_2MoS_4$ in oleylamine.[19] However, the structure, morphology, size and thickness are not controllable, and the design and engineering of structures of MoS_2 with exposed edge sites still remains a huge challenge.[6,20–22] Very recently, chemical vapor deposition (CVD) has been successful in growing high-quality graphene, and several groups have used it to synthesize MoS_2 thin films on 2D insulating substrates such as SiO_2 and sapphire.[3,23,24] Here, we report the first synthesis of MoS_2 nanosheets on 1D conductive CNFs by the CVD method, demonstrating the rational design and engineering of MoS_2 layered structures, and realizing the construction of structure-sensitive properties for HER with low overpotential and small Tafel slope. Moreover, by incorporating MoS_2 into a large nanostructured conductive substrate and a membrane electrode, we have successfully minimized the charge and mass transport limitations, lowering the resistivity of the MoS_2 crystal.

We first synthesized the CNF mats by combining the electrospinning and carbonization processes, and then the CNF mats were used as the substrate for the direct growth of MoS_2 nanocrystals *via* the CVD method. The synthesis strategy for hierarchical MoS_2–CNF nanomaterials is schematically illustrated in Fig. 1. In brief, MoO_3 powder was first thermally evaporated and reduced by sulfur vapor in the gas phase at 700–900 °C, and then the resulting MoO_2 was nucleated on the surfaces of the CNFs and grown into tubular shells along the entire CNF in a CVD furnace (see details in ESI†). The MoO_2 tubular shells were then annealed in sulfur vapor carried by Ar at 900 °C for 6 h. Because of the high-temperature annealing, the surface of the MoO_2 shells was sulfurized to MoS_2, with varying numbers of layers depending on the annealing duration. A series of morphological evolutions of MoS_2–CNF nanomaterials can be obtained, namely (i) bicontinuous MoS_2 scrolls with controlled layers grown around the CNFs, (ii) small 2D MoS_2 nanosheets grown on the MoS_2 scrolls along the CNFs, and (iii) 3D rose-petal-shaped MoS_2 nanosheet-CNFs hierarchical nanomaterials with controlled layers and a high density of exposed edges.

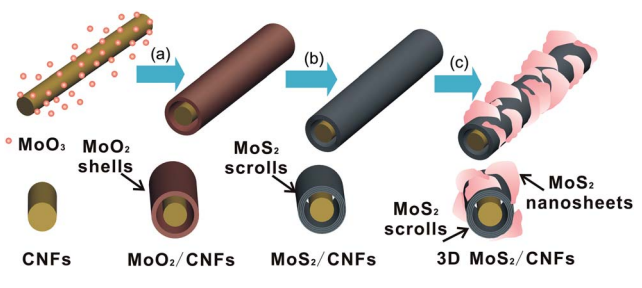

Fig. 1 Synthesis procedure for hierarchical MoS_2–CNF nanomaterials. (a) The nucleation of MoO_2 along the CNFs and the formation of MoO_2 shells; (b) the formation of MoS_2 scrolls after surface sulfurization by S vapor; (c) the growth of 2D MoS_2 nanosheets around the whole MoS_2 scroll-CNFs to form 3D architectures.

Results and discussion

Distinct and continuous PAN nanofibers with random orientation were obtained through the electrospinning process (Fig. S1a†). The PANFs, with smooth surfaces and uniform diameter of 525 ± 52 nm (Fig. S2a†), are up to hundreds of micrometers in length, leading to high surface-to-volume ratios. After carbonization treatment at 1000 °C, the diameter of the CNFs significantly reduces to 215 ± 48 nm (Fig. S2b†) and the continuous nanofibers can still be up to several tens of micrometers in length (Fig. S1b†). As shown by field emission scanning electron microscopy (FE-SEM) and transmission electron microscopy (TEM) in Fig. 2a and b, large-scale MoS_2 ultra nanosheets are grown along the CNFs to form continuous 3D rose-petal-shaped nanostructures. Fig. 2a and low-magnification FE-SEM images (Fig. S3†) clearly show that uniform and continuous 3D rose-petal-shaped MoS_2 nanosheets were grown along the whole CNF substrate and on nanofibers up to several hundred micrometers in length.

Fig. 2b also illustrates that the CNFs are completely covered by the MoS_2 nanosheets; the size of the nanosheets is several

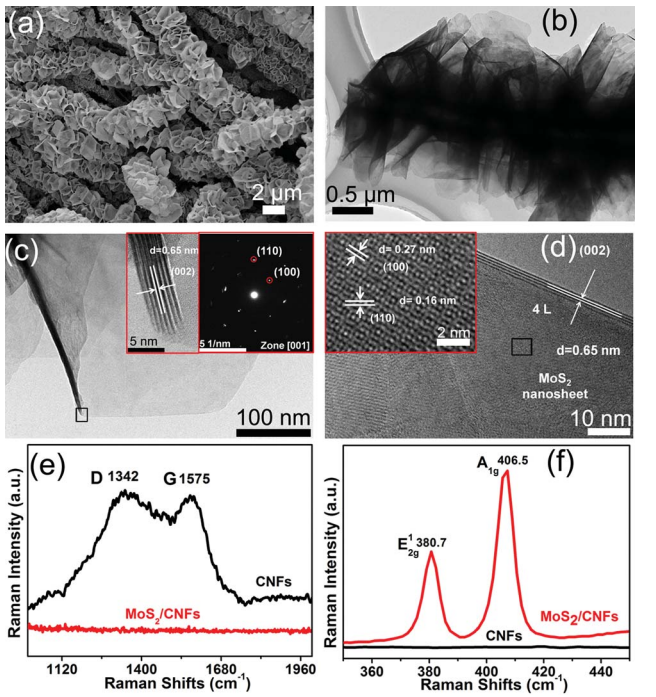

Fig. 2 (a) FE-SEM and (b) TEM image of MoS_2–CNF hierarchical nanomaterials. (c and d) TEM images of the rose-petal-shaped MoS_2 nanosheets. Inset in (c): SAED pattern of the MoS_2 nanosheet shown in (c) and HRTEM image of the MoS_2 wrinkle taken on the area marked in the rectangle in (c). Inset in (d): HRTEM image of the MoS_2 nanosheet taken on the area marked in the rectangle in (d). (e and f) Raman spectra of the CNF and hierarchical MoS_2–CNF nanomaterials.

micrometers (Fig. 2c). To verify the number of layers of MoS_2 nanosheets, we imaged the folded edges randomly taken on the nanosheets and observed four parallel dark lines with a spacing of 0.65 nm (Fig. 2d). In addition, we also imaged the wrinkled part of the MoS_2 nanosheets and eight parallel dark lines were observed (inset in Fig. 2c). These images confirm the layers of the rose-petal-shaped MoS_2 nanosheets. The inset in Fig. 2c displays the selected area electron diffraction (SAED) pattern taken on a single MoS_2 nanosheet, indicating the highly crystalline structure. The high-resolution TEM image of the MoS_2 nanosheet shows a honeycomb arrangement of the atoms with lattice spacing of 0.16 and 0.27 nm, corresponding to the (110) and (100) planes. Meanwhile, some disordered graphene-like hexagonal lattices emerged because of the mis-orientated stacking of Mo and S pairs in multilayer structures. Raman spectroscopy was further used to confirm the complete sulfurization of the MoS_2 from MoO_2. Fig. 2e shows the Raman spectra of pure CNF and MoS_2–CNF hierarchical nanomaterials. Two Raman peaks in the range of 1000–2000 cm^{-1} under 514 nm excitation were assigned to the D and G bands of carbon (1342 and 1575 cm^{-1}). After vapor growth and surface sulfurization, as shown in Fig. 2f the as-prepared MoS_2–CNF hierarchical nanomaterials have two distinct Raman peaks located at 380.7 (E_{2g}) and 406.5 (A_{1g}) cm^{-1}, respectively. The Raman spectrum of the MoS_2–CNFs in the range of 1000–2000 cm^{-1} did not show any peaks of carbon, indicating that MoS_2 nanosheets completely covered the CNFs. In order to verify the reproducibility of the synthesized MoS_2–CNF mats, we measured ten samples of Raman spectra of the MoS_2–CNF mats, and the results exhibit similar Raman peaks of MoS_2 (Fig. S4†).

X-ray photoelectron spectroscopy (XPS) was employed to investigate graphitization of the CNFs from PANFs and the chemical states of Mo and S in the MoS_2–CNF nanomaterials. Fig. 3a and b show the XPS spectra of C 1s and N 1s of the PANFs and the CNFs after graphitization at 1000 °C under an Ar protecting environment. The C 1s spectrum of the PANFs displays two peaks with binding energies at 284.7 and 285.8 eV, which accord with the carbon atoms in C–C bonds and C≡N bonds, respectively. After thermal annealing at 1000 °C, the CNFs only exhibit one sharp peak located at 284.7 eV (C–C bonds), indicating the formation of graphitic CNFs. For the PANFs, the N 1s spectrum depicts a strong peak located at 398.8 eV, and it can be assigned to the nitrogen atoms that bond with carbon atoms in the form of C≡N (Fig. 3b).[15] On the sample CNFs, two weaker N 1s peaks emerged at 398.8 eV and 401.2 eV. The former is ascribed to the C≡N species as mentioned above, while the latter is attributed to pyridine type nitrogen. In addition, the weak intensity of the N 1s peaks demonstrates that most of the nitrogen vanishes after the carbonization process. Fig. 3c and d show the XPS spectra of Mo 3d and S 2p of the 3D rose-petal-shaped MoS_2 ultra nanosheets grown on the continuous scrolled MoS_2–CNFs. The Mo 3d orbit of the MoS_2–CNFs exhibits two peaks located at 229.1 and 232.2 eV, which are ascribed to the doublet of Mo $3d_{5/2}$ and Mo $3d_{3/2}$, respectively (Fig. 3a).[23–25] The binding energies for S $2p_{3/2}$ and $2p_{1/2}$ were 162.5 and 163.2 eV, respectively (Fig. 3d). These measured binding energies of Mo and S accord with the MoS_2 crystals. X-ray diffraction (XRD) patterns of the CNF and MoS_2–CNF hybrid fibrous mats were obtained to investigate the crystalline phase compositions. As shown in Fig. S5,† the CNFs display the representative diffraction peak (002) of the stacked graphite layers at 25.2° and the *d*-spacing of CNFs is $d(002) = 3.52$ Å, indicating the crystalline structure of graphitic carbon in the nanofibers.[26,27] Besides the (002) peaks of the CNFs, the MoS_2–CNF nanomaterials exhibit four new peaks at 14.9°, 34.3°, 40.4° and 60.3°, and they are ascribed to the (002), (100), (103) and (100) crystal planes, respectively, indicating MoS_2 crystal domains with hexagonal structure [(PDF) no. 771716].[24,25] The strong intensity of (002) planes of MoS_2 displays the high density of exposed edge sites.

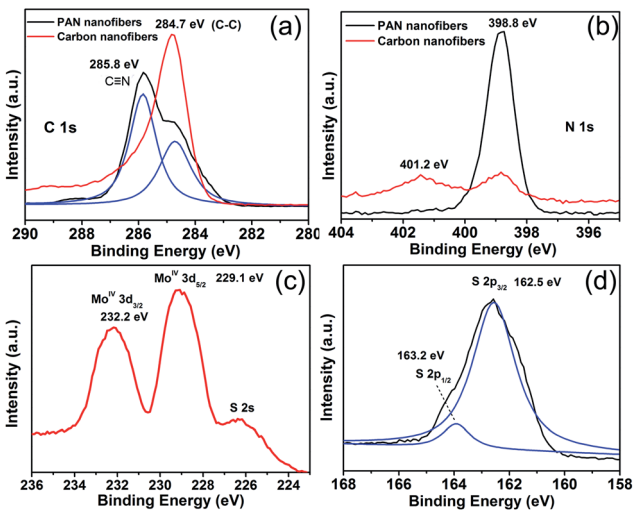

Fig. 3 XPS spectra of C 1s (a) and N 1s (b) of the PAN and carbon nanofibers. XPS spectra of Mo 3d (c) and S 2p (d) of the MoS_2–CNF hierarchical nanostructure.

By changing the amounts of MoO_3, a series of morphological evolutions can be obtained. At low amounts of MoO_3, as shown in Fig. 4a and d, the rough CNFs are completely covered by layers of MoS_2 nanosheets, and several small isolated 2D MoS_2 nanosheets grow on the layered nanosheets along with the CNFs. With increasing amounts of MoO_3, small 2D MoS_2 nanosheets appear and the density of nanosheets increases throughout the CNF (Fig. 4b and e). At the highest amounts, 2D MoS_2 nanosheets grow throughout the MoS_2-coated CNFs to produce 3D continuous MoS_2–CNF hierarchical nanomaterials (Fig. 4c and f). The 2D rose-petal-shaped MoS_2 nanosheets grow densely and uniformly along with the CNFs. Based on the above results, different morphologies of the MoS_2–CNFs can be easily obtained by adjustment of the amount of MoO_3. The carbonaceous matrix of CNFs consisted of small and random graphene layers (Fig. S6†). As shown in the TEM images, at 0.020 g of MoO_3 it is clearly observed from the edge of the MoS_2–CNFs that a MoS_2 scroll with about 20 layers is assembled around the whole CNF. The well-defined layered structure of the MoS_2 scroll has an interlayer distance of 0.65 nm for (002) planes (inset in Fig. 4d). In addition, the phenomenon of wrinkled MoS_2 nanosheets on the surface of the CNF indicates that the CNF substrates were encapsulated in the MoS_2 scrolls.

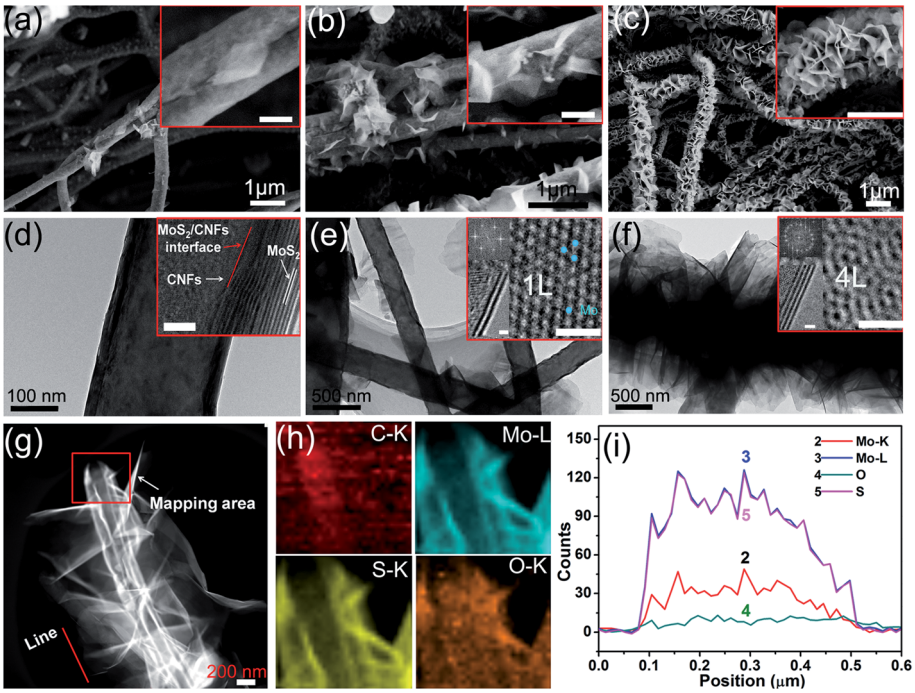

Fig. 4 (a) FE-SEM and TEM images of the morphological evolutions of MoS_2–CNFs with different amounts of MoO_3: (a and d) 0.020 g, (b and e) 0.035 g and (c and f) 0.05 g. Insets in (a–c) are high-magnification FE-SEM images of MoS_2–CNFs (scale bar, 100 nm). The inset in (d) is a HRTEM image of the edges of the scrolled MoS_2–CNFs (scale bar, 5 nm). Insets in (e–f) are HRTEM images of the MoS_2 nanosheets, the folded MoS_2 edges, and the corresponding FFT patterns (scale bar, 1 nm). HAADF-STEM images (g) and STEM-EDX element mappings (h) taken on the scrolled MoS_2–CNFs. (i) Line-scan EDX spectra taken on the MoS_2 nanosheets grown on the MoS_2 scroll-CNFs.

As amounts were continuously increased to 0.020 g, small 2D MoS_2 nanosheets began to grow on the surfaces of the MoS_2 scrolls (Fig. 4e). The HRTEM image shown in Fig. 3e exhibits the honeycomb arrangements of the Mo and S atoms, and the folded edges of the MoS_2 nanosheet presents one dark fringe with a space of ~0.65 nm, confirming the bilayer nanostructure of MoS_2. The light spots are ascribed to Mo atoms (blue). The fast Fourier transform (FFT) also shows the hexagonal symmetry of the MoS_2 structure. When the amount was increased to 0.05 g, large 2D MoS_2 nanosheets grew densely and uniformly on the scroll MoS_2–CNF substrates (Fig. 4f). As shown in the insets of Fig. 4f, the HRTEM image of the rose-petal-shaped MoS_2 nanosheets displays a disordered hexagonal structure and the folded edges of the MoS_2 nanosheets present four dark fringes, confirming the multilayer nanostructure of MoS_2. Shi *et al.*[21] have reported that the arrangement of the atoms can reflect the layer structures. If the MoS_2 domains have a layer number ≥2, both AB stacking and mis-orientated stacking would emerge.

The AB stacking bilayer region in Fig. 4e shows uniform intensity for the hexagonal lattice due to the overlapping of the Mo and S pairs in the top and bottom layers. With increasing number of layers, for example 4 layers, the orientation of the atoms becomes disordered and the FFT patterns also confirm the mis-orientated stacking (insets in Fig. 4f). Therefore, along with the growth of 2D MoS_2 nanosheets from small to larger size, the number of layers also increased from 1 layer to 4 layers.

Fig. 4g shows a high-angle annular dark field scanning TEM (HAADF-STEM) image of the 3D MoS_2–CNF nanomaterials. The MoS_2 scrolls can be clearly observed and the STEM-EDX mapping of Mo and S elements indicates the semi-hollow structure of the MoS_2 scrolls. The STEM-EDX mapping displays four different elements and the red, blue, yellow and orange regions in the images correspond to the elements C, Mo, S and O. In the mapping of C (Fig. 4h), the dense signal area belongs to the CNFs and the other C signals are ascribed to the carbon-coated Cu grid. The line-scan EDX spectrum of the 2D MoS_2 nanosheet demonstrates the strong Mo and S signals and the very much weaker O signal, indicating complete sulfurization from MoO_2 to MoS_2. The Raman spectra of the three samples also provide evidence for the morphological evolutions (Fig. S7†). The scrolled MoS_2–CNF (sample a) exhibits four distinct Raman peaks, which are ascribed to E_{2g} and A_{1g} of MoS_2 and the D and G bands of carbon. With the morphological evolution of the MoS_2–CNF architecture, the intensities of the peaks of MoS_2 increase and the D and G bands of carbon decrease. The Raman spectra of the 3D MoS_2–CNF nanomaterials did not display the D and G bands of carbon, demonstrating that the CNFs are densely covered by the MoS_2 nanosheets.

The morphological evolution of 3D hierarchical MoS_2–CNF nanomaterials brings us a promising way to design and engineer surface structures at the nanoscale, which is paramount in developing effective catalysts. In order to show the structure-sensitive properties of the MoS_2–CNF hierarchical nanomaterials, we evaluated the electrochemical activity of the scrolled MoS_2–CNFs (sample a), the small 2D MoS_2 nanosheets grown on the scrolled MoS_2–CNFs (sample b), and the 3D MoS_2–CNF

nanomaterials (sample c) for the HER. An excellent catalyst for the HER should reduce the overpotential and consequently increase the efficiency of this important electrochemical process, depending on the highly catalytic edge sites of the MoS_2 nanosheets.[7,8,25] In our systems, the constructed 3D rose-petal-shaped MoS_2 nanosheets grown on the scrolled MoS_2–CNFs can offer densely exposed active edge sites for HER. The direct growth of MoS_2 nanosheets on conducting CNF substrates enabled a convenient evaluation of their catalytic activity by attachment of the MoS_2–CNF mats to electrode holders in 0.5 M H_2SO_4 solution using a typical three-electrode setup (see ESI† for details). As shown in Fig. 5A, the polarization curves (i–V plot) recorded with our three samples showed overpotentials of ~0.2 V (sample d), 0.15 (sample e), and 0.12 V (sample f), respectively. In addition, the linear portions of the Tafel plots (Fig. 5B) were fit to the Tafel equation ($\eta = b \log j + a$, where j is the current density and b is the Tafel slope).[7,8] The Tafel slopes of the three samples are ~160, ~97, and ~45 mV per decade, respectively. As a control experiment, the HER activity of pure CNFs (sample a), MoS_2 powder (sample b) and a mixture of MoS_2 powder and CNFs (sample c) were also examined. As shown in Fig. 5, the samples show much lower activity and current density than the MoS_2–CNF hierarchical nanostructures. In addition, sample f, in comparison with the other samples, exhibits the lowest overpotential and Tafel slope because of the large numbers of exposed edge sites, demonstrating excellent HER activity. Note that a trend can be clearly observed, with the morphological evolutions along with increased amounts of exposed edge sites leading to smaller Tafel slopes.

The high electrocatalytic activity of the hierarchical MoS_2–CNF hybrid catalysts in the HER is attributed to the strong chemical and electronic coupling between the conducting CNFs and the MoS_2 nanosheets with various structures. Unlike the deposition of catalysts on conducting substrates, such as Ni foams and graphene, the CNFs serve as the nucleation sites and templates for growth of MoS_2 scrolls and rose-petal-shaped 3D MoS_2 nanosheets. Chemical coupling helps the direct growth of highly uniform MoS_2 around the CNFs to form scrolls and rose-petal-shaped nanosheets. Electrical coupling to the underlying CNFs in an interconnected conducting network affords rapid electron transport from the less-conducting MoS_2 nanosheets to the electrodes. To measure this effect and verify the strong chemical and electrical coupling, an electrochemical impedance measurement at an overpotential of $\eta = 0.12$ V was performed (Fig. S8†). In a control experiment, the pure CNFs, bulk MoS_2 powder and mixture of MoS_2 powder and CNFs show charge-transfer resistance (R_{CT}) of ~3.5 kΩ (sample a), 10 kΩ (sample b), and 8 kΩ (sample c), respectively. However, the MoS_2–CNF nanomaterials (from sample d to f) exhibit much lower R_{CT} of ~300, ~150 and ~45 Ω, supporting the strong chemical and electrical coupling effects. The remarkable decrease of Z_f offers markedly faster HER kinetics with the MoS_2–CNF hybrid catalysts.

Besides HER activity, high durability is another important criterion for a good catalyst. To evaluate the stability in an acidic environment, we cycled the hierarchical MoS_2–CNF mats (sample c) continuously for 1000 cycles. After the continuous operation, the MoS_2–CNFs showed a 5% decay in the electrocatalytic current density (Fig. S9†), suggesting the high stability of the electrocatalyst based on MoS_2–CNF mats during long-term cycling. Compared with Pt-based electrocatalysts, the activity of the present MoS_2–CNF nanomaterials must still be further improved. However, due to the high costs of Pt, the results of the present investigation provide a promising alternative for the production of hydrogen energy.

Conclusions

In summary, we have synthesized large-scale continuous hierarchical MoS_2–CNF nanomaterials with highly exposed edge site architecture of MoS_2, with tunable structures from 1D scrolls to 2D nanosheets that exhibit structure-sensitive properties for the HER. By controlling the MoS_2 morphology at the nanoscale, we have produced evolutions in the structure and preferentially exposed more catalytically active edge sites, enabling improved performance for electrochemical catalytic activity. Because of the highly exposed edges and excellent chemical and electrical coupling to the underlying CNFs, the MoS_2–CNFs nanofiber mats exhibited excellent HER activity with a small overpotential of ~0.12 V and small Tafel slope of 45 mV per decade. The construction of structure-sensitive nanomaterials with enhanced HER activity provide a feasible way to design and engineer advanced nanostructures for catalysis, electronic devices and other potential applications.

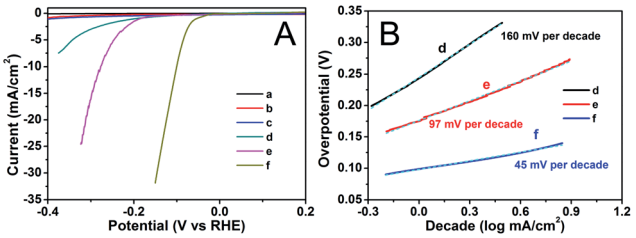

Fig. 5 Electrocatalytic activities of hierarchical MoS_2–CNF nanomaterials for the hydrogen evolution reaction. (A) Polarisation curves obtained with different morphologies of MoS_2–CNF nanomaterials: (a) CNFs, (b) MoS_2 powder, (c) mixture MoS_2 powder and CNFs, (d) scrolled MoS_2–CNFs, (e) small 2D MoS_2 nanosheets grown on the scrolled MoS_2–CNFs and (f) 3D MoS_2–CNF nanostructures. (B) The corresponding Tafel plots of the three samples (d–f).

Acknowledgements

This work was supported by the National Natural Science Foundation of China (NSFC) (51373154) and the 521 Talent Project of Zhejiang Sci-Tech University.

Notes and references

1 J. Kibsgaard, Z. B. Chen, B. N. Reinecke and T. F. Jaramillo, *Nat. Mater.*, 2012, **11**, 963–969.
2 Z. Y. Wang, H. Li, Z. Liu, Z. J. Shi, J. Lu, K. Suenaga, S. K. Joung, T. Okazaki, Z. N. Gu, J. Zhou, Z. X. Gao, G. P. Li, S. Sanvito, E. G. Wang and S. Iijima, *J. Am. Chem. Soc.*, 2010, **132**, 13840–13847.

3 K. Yan, L. Fu, H. L. Peng and Z. F. Liu, *Acc. Chem. Res.*, 2013, **46**, 2263–2274.
4 M. S. Choi, G. H. Lee, Y. J. Yu, D. Y. Lee, S. H. Lee, P. Kim, J. Hone and W. J. Yoo, *Nat. Commun.*, 2013, **4**, 1624–1630.
5 T. F. Jaramillo, K. P. Jorgensen, J. Bonde, J. H. Nielsen, S. Horch and I. Chorkendorff, *Science*, 2007, **317**, 100–102.
6 J. N. Coleman, M. Lotya, A. O'Neill, S. D. Bergin, P. J. King, U. Khan, K. Young, A. Gaucher, S. De, R. J. Smith, *et al.*, *Science*, 2011, **331**, 568–571.
7 M. A. Lukowski, A. S. Daniel, F. Meng, A. Forticaux, L. S. Li and S. Jin, *J. Am. Chem. Soc.*, 2013, **135**, 10274–10277.
8 Y. G. Li, H. L. Wang, L. M. Xie, Y. Y. Liang, G. S. Hong and H. J. Dai, *J. Am. Chem. Soc.*, 2011, **133**, 7296–7299.
9 J. F. Xie, J. J. Zhang, S. Li, F. Grote, X. D. Zhang, H. Zhang, R. X. Wang, Y. Lei, B. C. Pan and Y. Xie, *J. Am. Chem. Soc.*, 2013, **135**, 17881–17888.
10 T. F. Jaramillo, J. Bonde, J. D. Zhang, B. L. Ooi, K. Andersson, J. Ulstrup and I. Chorkendorff, *J. Phys. Chem. C*, 2008, **112**, 17492–17498.
11 Y. B. Chen, Z. Y. Shen, Z. W. Xu, Y. Hu, H. T. Xu, S. Wang, X. L. Guo, Y. F. Zhang, L. M. Peng, F. Ding, Z. F. Liu and J. Zhang, *Nat. Commun.*, 2013, **4**, 2205–2210.
12 Q. Qing, D. A. Nezich, J. Kong, Z. Y. Wu and Z. F. Liu, *Nano Lett.*, 2010, **10**, 4715–4720.
13 Z. F. Liu, L. Y. Jiao, Y. G. Yao, X. J. Xian and J. Zhang, *Adv. Mater.*, 2010, **22**, 2285–2310.
14 D. Jariwala, V. K. Sangwan, L. J. Lauhon, T. J. Marks and M. C. Hersam, *Chem. Soc. Rev.*, 2013, **42**, 2824–2860.
15 W. Li, L. S. Zhang, Q. Wang, Y. Yu, Z. Chen, C. Y. Cao and W. G. Song, *J. Mater. Chem.*, 2012, **22**, 15342–15347.
16 L. Matlock-Colangelo and A. Baeumner, *Lab Chip*, 2012, **12**, 2612–2620.
17 H. Q. Hou and D. H. Reneker, *Adv. Mater.*, 2004, **16**, 69–73.
18 A. Greiner and J. H. Wendorff, *Angew. Chem., Int. Ed.*, 2007, **46**, 5670–5703.
19 I. Zafiropoulou, M. S. Katsiotis, N. Boukos, M. A. Karakassides, S. Stephen, V. Tzitzios, M. Fardis, R. V. Vladea, S. M. Alhassan and G. Papavassiliou, *J. Phys. Chem. C*, 2013, **117**, 10135–10142.
20 K. Chang and W. X. Chen, *ACS Nano*, 2011, **5**, 4720–4728.
21 Y. M. Shi, Y. Wang, J. I. Wong, A. Y. S. Tan, C. L. Hsu, L. J. Li, Y. C. Lu and H. Y. Yang, *Sci. Rep.*, 2013, **3**, 2169–2176.
22 X. S. Wang, H. B. Feng, Y. M. Wu and L. Y. Jiao, *J. Am. Chem. Soc.*, 2013, **135**, 5304–5307.
23 K. K. Liu, W. J. Zhang, Y. H. Lee, Y. C. Lin, M. T. Chang, C. Y. Su, C. S. Chang, H. Li, Y. M. Shi, H. Zhang, C. S. Lai and L. J. Li, *Nano Lett.*, 2012, **12**, 1538–1544.
24 X. W. Mao, F. Simeon, G. C. Rutledge and T. A. Hatton, *Adv. Mater.*, 2013, **25**, 1309–1314.
25 M. Chhowalla, H. S. Shin, G. Eda, L. J. Li, K. P. Loh and H. Zhang, *Nat. Chem.*, 2013, **5**, 263–275.
26 S. B. Lee, S. B. Son, K. M. Park, G. Lee, K. H. Oh, S. H. Lee and W. R. Yu, *ACS Appl. Mater. Interfaces*, 2012, **4**, 6702–6710.
27 Y. M. Shi, W. Zhou, A. Y. Lu, W. J. Fang, Y. H. Lee, A. L. Hsu, S. M. Kim, K. K. Kim, H. Y. Yang, L. J. Li, J. C. Idrobo and J. Kong, *Nano Lett.*, 2012, **12**, 2784–2791.